LEGIBILITY NOTICE

A major purpose of the Technical Information Center is to provide the broadest dissemination possible of information contained in DOE's Research and Development Reports to business, industry, the academic community, and federal, state and local governments.

Although a small portion of this report is not reproducible, it is being made available to expedite the availability of information on the research discussed herein.

LA-UR -90-2571

LA-UR--90-2571

DE90 014979

TITLE Numerical Models of 2-D and 3-D Geophysical Convection

AUTHOR(S) Bryan J. Travis

SUBMITTED TO ASME Winter Annual Meeting, Session on Heat Transfer in Earth Science Studies, Dallas, Texas, November 25-30, 1990

DISCLAIMER

Los Alamos Los Alamos National Laboratory
Los Alamos, New Mexico 87545

Numerical Models of 2-D And 3-D Geophysical Convection

Bryan J. Travis
Earth and Environmental Sciences Division
MS-F665
Los Alamos National Laboratory
Los Alamos, NM 87545, USA

ABSTRACT

A suite of computational models has been developed which simulate thermal/chemical convection over a wide range of Rayleigh numbers both in 2- D annular and 3-D Cartesian geometries, for small Reynolds number flow, and a variety of boundary conditions. These simulators are revealing the patterns of convection that may occur in the earth, from mantle scale down to more localized regions such as mid-ocean spreading centers, on down to the scale of magma chambers. Features such as surface plates, variable viscosity and chemical buoyancy can have a dramatic impact on convective patterns compared to those seen in simple, constant property, free or fixed surface systems. In most cases, the nonlinear dynamics of these systems derive from thermal and chemical forces, rather than inertial. These models can be used to study general features and dynamics of convecting viscous fluids, and can also be used to constrain possible explanations for geophysical observations such as heat flow, gravity, topography, plate speeds, and isotopic distributions. Computational resources have reached a level at which numerical solutions of complex processes are feasible.

NOMENCLATURE

g	gravitational acceleration	m/s^2
r	radius	m
t	time	sec
u	horizontal velocity in x direction in 3 D, radial velocity in 2 D	m/s
v	horizontal velocity in y direction in 3 D, azimuthal velocity in 2 D	m/s
w	vertical velocity in z direction in 3 D	m/s
x	spatial dimension	m
A	mesh cell face area	m^2
B	ratio of chemical to thermal buoyancy	
C	concentration	kg/kg
H	depth of system	m
Q	correction terms to cancel $0(\Delta t)$ error	
T	temperature	°C
$\dot{D}$	rate of heat production from radioactive decay	s^{-1}
D_c	molecular diffusivity	m^2/s
L_e	Lewis number	
N_f	number of faces on a mesh cell	
R_a	Rayleigh number	
$\vec{u}$	velocity vector	m/s
α	thermal expansivity	m/m
κ	thermal diffusivity	m^2/s
ν	kinematic viscosity	m^2/s
ρ	density	kg/m^3
ρ_0	reference density	kg/m^3
ρ_1	density of upper layer	kg/m^3
ρ_2	density of lower layer	kg/m^3
θ	angular dimension	°
Δt	time step size	sec
$\Delta\rho$	density difference	kg/m^3
$\Delta\Omega$	mesh cell volume	m^3
Γ	velocity potential for 3-D model	m^2/s
Ψ	stream function for 2-D model	m^2/s

INTRODUCTION

Fluid flow systems of geophysical interest include convection in the mantle with tectonic plates and chemical heterogeneity, convection beneath mid ocean ridges, and convection within magma bodies. Other systems involving creeping flow include

subduction of slabs with subsequent delamination. In each of these cases, the flow is slow, ie, essentially inertialess, but the thermal and chemical structure may be complex, e.g., high Rayleigh number and presence of two or more species. Usually, analytical solutions for the governing equations are not available and numerical approximations are used.

Well-conceived numerical methods are required to adequately resolve the transient, turbulent or highly convoluted flow patterns and temperature/concentration structures that can develop in these models. There are several numerical approximation methods that can be used, e.g., finite differences, finite elements, adaptive meshes, the Lagrangian approach, or spectral representations. The approach taken here is to use front tracking schemes in conjunction with high-order finite difference and spectral methodologies. Finite differences are fairly simple compared to the other approaches, and can be highly accurate if done carefully. Front tracking methods can follow sub-scale structure or irregularly shaped features such as subducting slabs that may not move in a direction that is aligned with computational zones and are difficult for finite differences to treat. Together, these methods provide a very powerful way of simulating complex flows. This paper will describe the finite difference and front tracking algorithms used, and present three applications.

MODEL

The governing equations for creeping flow with chemical stratification are listed and described here. This treatment neglects complications such as temperature dependent viscosity; such features lead to an additional set of considerations for numerical methods. The emphasis in this short paper is on convecting systems of immiscible species with and without plates.

For a two species, isoviscous flow subject to a Boussinesq approximation for thermal and chemical buoyancy, a stream function, vorticity formulation can be used, resulting in the following equation set (see, e.g., Christensen and Yuen, 1984):

for 2-D annulus

$$\nabla^4\Psi = R_a\left(\frac{\partial T}{r\partial\theta} - B\frac{\partial C}{r\partial\theta}\right) \tag{1}$$

$$u = \frac{\partial\Psi}{r\partial\theta}, \quad v = \frac{\partial\Psi}{\partial r} \tag{2}$$

for 3-D cartesian geometry,

$$\nabla^4\Gamma = R_a\left(\frac{\partial T}{\partial x} - B\frac{\partial C}{\partial x}\right) \tag{3}$$

$$u = \frac{\partial\Gamma}{\partial z\partial y}, \quad v = \frac{\partial\Gamma}{\partial z\partial y}, \quad w = \left(\frac{\partial^2\Gamma}{\partial x^2} + \frac{\partial^2\Gamma}{\partial y^2}\right) \tag{4}$$

where thermal Rayleigh number $R_a = \alpha\rho_0 g\Delta T H^3/\kappa\nu$ and $B = \Delta\rho/\rho/\alpha\Delta T$ is the ratio of chemical to thermal buoyancy, T is temperature, C is concentration, Ψ is the stream function in 2-D, Γ is the velocity potential in 3-D, α is thermal expansion coefficient, and $\Delta\rho = \rho_1 - \rho_2$, the difference in density between the two species, ΔT is temperature difference between top and bottom surfaces, g is gravity, H is depth of the system, κ is thermal diffusivity, and ν is kinematic viscosity.

Density is given by

$$\rho = \rho_0\left((1 - \alpha\Delta T\cdot T + \frac{\Delta\rho}{\rho}\cdot C\right) \tag{5}$$

The non-dimensional energy equation in conservative form is

$$\frac{\partial T}{\partial t} + \nabla\cdot(\vec{u}T) = \nabla^2 T + \dot{D} \tag{6}$$

where $\dot{D}$ is the rate of heat production from radioactive decay. For an incompressible fluid, the conservation equation of species is -

$$\frac{\partial C}{\partial t} + \nabla\cdot(\vec{u}C) = \frac{D_C}{\kappa}\nabla^2 C \tag{7}$$

where D_C is material diffusivity, on the order of 10^{-12} m^2/s (Hoffman and Magaritz, 1977) or less in the earth's mantle, and κ is on the order of 10^{-6} m^2/s (McKenzie, Roberts and Weiss, 1974), so that the right hand side of eqn. (7) is negligible, and the equation is essentially an advective transport equation. The ratio D_C/κ is $1/Le$, where Le is the Lewis number.

NUMERICAL SOLUTION

The region of interest is first divided into a uniform mesh of cells. Present practical limit on the maximum size of a mesh is about 500,000 cells on a CRAY-XMP. More can be used, but only if hardware such as solid state disks or a very large computer such as a CRAY-YMP are available. The solution of equations (1) and (3) is relatively straight forward. In 2-D, Eqn (1) is used. It is Fourier transformed in the θ direction, leaving a coupled pair of second order ordinary differential equations for each wave number. Centered differencing of these equations results in a set of tridiagonal matrix equations, which can be solved very fast. A back transform is then executed to get the stream function and then the velocity. In 3-D, Eqn (3) is transformed twice, first in the x dimension, then in the y dimension, resulting in a 4th order ordinary differential equation for each wave number pair. Centered differencing results in a pentadiagonal matrix equation to solve for each wave number pair. The solution of these are back transformed to obtain Γ and then the velocities. The temperature solution, Eqn (6), is strictly finite difference forward in time, and integrated in space, with a tensor diffusivity to cancel numerical dispersion.

The finite difference analogue of Eqn. (6) for temperature is

$$T_{ijk}^{n+1} = T_{ijk}^{n} + \frac{\Delta t}{\Delta\Omega}\sum_{1}^{N_f}\left(-\int_0^1 \vec{u}\hat{T}\cdot dA + \int_0^1 \nabla T\cdot dA + \frac{\Delta t}{2}\int_0^1 \vec{u}Q\cdot dA\right)^n + \dot{D} \qquad (8)$$

where $Q = \nabla\cdot\vec{u}T$, and N_f is the number of faces (4 for 2-D, 6 for 3-D) on a cell, $\Delta\Omega$ is the volume of a cell, A is cell face area, superscript n refers to time level, and subscript ijk refers to cell location. The integrals on the right hand side of Eqn. (8) are evaluated at time level n over each face of a computational cell. The last integral term on the right hand side of Eqn. (8) is required to make the finite difference form approach the solution of the differential equation. It is a corrector term to cancel $O(\Delta t)$ error introduced by forward time differencing (Hirt, 1968) of the lefthand side of Eqn. (6). It cancels (almost) the numerical diffusion introduced by the finite difference form and provides approximately $O(\Delta t^2)$ accuracy (Ramshaw and Dukowicz, 1979; Margolin and Smolarkiewicz, 1989). The integration of the first integral on the right requires special treatment. Over each cell face, velocity is a bilinear function between the values at cell corners, and temperature is a quadratic. The form for $\hat{T}$ in 2-D annular geometry over a face perpendicular to a radius is

$$\hat{T} = \hat{T}_i\left(\frac{\Delta r}{2} + u(\theta)\cdot\Delta t\right) + \hat{T}_{i+1}\left(\frac{\Delta r}{2} - u(\theta)\cdot\Delta t\right) \qquad (9)$$

$$\hat{T}_i = \theta T_{i,j+1} + (1-\theta)T_{ij} \qquad (10)$$

where θ is fractional distance in the azimuthal direction from node j to node $j+1$, Δr is cell width in the direction perpendicular to θ, i indicates cell number in the r direction and j in the θ direction, and u is lineu in θ. A completely analogous expression is used over faces in the perpendicular direction. This is a high order upwind scheme, consisting of a 9 point stencil in 2 D and a 27-point stencil in 3-D, and is very accurate, $O(\Delta x^4)$ (Roache, 1972), when used in Eqn. (8). The integration of Eqn. (8) is exact using two-point (in each dimension) Gaussian quadrature. In 3-D, Eqns. (9) and (10) acquire two dimensional dependency, but otherwise the approach is identical. An important feature of this solution is that mass and energy are conserved. This is frequently as important for accuracy as the formal truncation error (Roache, 1972)

If the Lewis number Le is not large, the advective diffusive Eqn (7) can be solved accurately using the same scheme as described for solving Eqn (6) For large Lewis number values, even that scheme will generate excessive numerical diffusion. We then treat the materials as essentially immiscible and use a front tracking scheme to follow the interface between the species

FRONT-TRACKING

The primary advantage of front tracking methods is that they can follow interfaces even when they becomes highly convoluted or disconnected. Here, highly deformable marker chains and marker surfaces are used to follow the evolution of convection in a system of two immiscible materials. In 2-D, the interface consists of a string of particles whose velocities are determined by interpolation from the velocity values computed at cell corners. Points can be added or deleted; strings can split or merge, so that a collection of arbitrarily shaped, disconnected regions can be followed. The criteria for adding and deleting points involve the separation between successive points and the local curvature. In 3-D, the interfaces consist of sheets of connected triangles. Rules for adding and subtracting triangles, and splitting and merging sheets are more involved than in 2-D, and include tests on the area and ratio of altitudes in each triangle (see, e.g., Dritschel, 1988; Schafer-Perini, Wilson and Perini, 1990; Schafer-Perini and Wilson, 1990). Forward and backward link lists are used to reduce computer memory and run time. Calculation of the concentration of each specie in each finite difference mesh cell is needed for the buoyancy term in Eqns. (1) and (3) and is determined by a careful calculation of the volume occupied by each specie in each mesh cell. This requires a tabulation of the parts of each chain or sheet that lie in each mesh cell. This approach greatly reduces the artificial mixing that occurs when using ordinary finite difference or finite element transport solutions. Examples of numerical solutions are presented now to illustrate these processes and solution methods.

EXAMPLES

(1) 3-D Convection – Effect of Plates and Internal Heating

Two of the most important features affecting mantle convection in the earth are the presence of surface plates and production of heat from decay of radioactive elements in the interior. Sample calculations are presented illustrating these effects. The first simulation treats tectonic plates; they are generally handled by applying a specified velocity field at the surface or by determining the shear stress on the surface and finding a self-consistent surface velocity form (Gable, 1989). In either case, a plate is an upper boundary condition modification. Plates control the scale of the underlying convecting system. Fig. 1 contrasts 3-D patterns with and without a surface plate. In both cases, a 1 x 3 x 3 box geometry was used, and a zoning of 24 x 72 x 72 mesh cells. The Rayleigh number was set at 10^5. In the first, a plate is specified, moving in the $+x$ direction at a speed of 500 (non dimensionalized, corresponds to a real speed of several cm/yr, in the range of actual plates). In the second, the upper surface is a free slip boundary. In both calculations, the bottom surface is free slip and the sides are reflective Initial conditions for both cases are a conductive temperature profile plus a random perturbation with maximum amplitude of 0.01. In Fig. 1, a hexagonal pattern is seen in the temperature structure. This is only one possible mode; the initial conditions are also important in determining the final pattern seen in 3 D geometries (see

Travis, Olson and Schubert, 1990). In Fig. 1, the flow field is completely different; it is now organized into long rolls parallel to the direction of motion of the plate. These long roll-like structures may provide a basis for explaining lineations seen in gravity maps of the large Pacific plate.

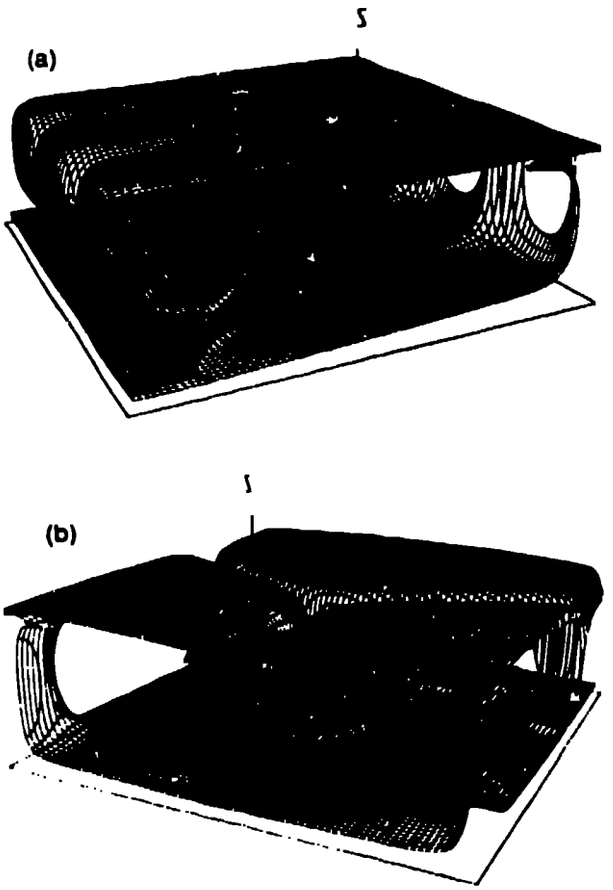

Fig. 1(a). Non-dimensional temperature surfaces of T=0.35 (upper surface) and T=0.75 (lower) for convection in a 1 x 3 x 3 box at Rayleigh number of 10^5 with surface plate. Plate is moving from right to left at velocity of 500 (non-dimensional). (b) Non-dimensional temperature surfaces of T=0.25 (upper) and T=0.75 (lower) under same conditions as (a) except that surface plate has been replaced by a free surface (no shear) condition. Flows in both cases have reached a steady state.

A second 3-D simulation is presented to show the large difference that internal heating can make on planforms. This simulation (Travis, Weinstein and Olson, 1990) was successfully compared to a laboratory experiment (Weinstein and Olson, 1990) and is therefore a code validation exercise as well. In this case, a geometry of a 1 x 3 x 3 box is used, with 28 x 84 x 84 mesh zones in the vertical and horizontal directions, respectively. The Rayleigh number based on bottom heating is 1.5×10^5. Upper and lower surfaces are no slip boundaries and sides are reflective. A calculation without internal heating was performed for comparison purposes. The resulting flow (Fig. 2a) consists of an almost steady, spoke-shaped pattern of connected upwelling and downwelling ridges, about equal in magnitude. The upwelling system is offset so that downwelling ridges are roughly perpendicular to the upwelling pattern. In the second calculation, internal heating was added to simulate radioactive decay in the earth's interior. The resulting flow pattern (Fig. 2b) is now very different; downwelling plumes and ridges form and breakup on a fairly rapid timescale. Upwelling is diffuse and poorly organized. The implication is that these ridges and downwelling plumes are important factors in controlling where and when plates subduct. Rayleigh number based on internal heating was 1.8×10^6. In the first simulation, a conductive profile with a 0.001 random perturbation was used as the initial temperature field. The second was started by setting $\dot{D}$ in Eqn. (6) to 12 at time 0.16 for the flow field of Case 1. The flow calculated in Figs. (2a) and (2b) agreed quite well with experimental observation, both in terms of the flow patterns seen and in terms of the rate of change of the patterns, providing a validation of the numerical model.

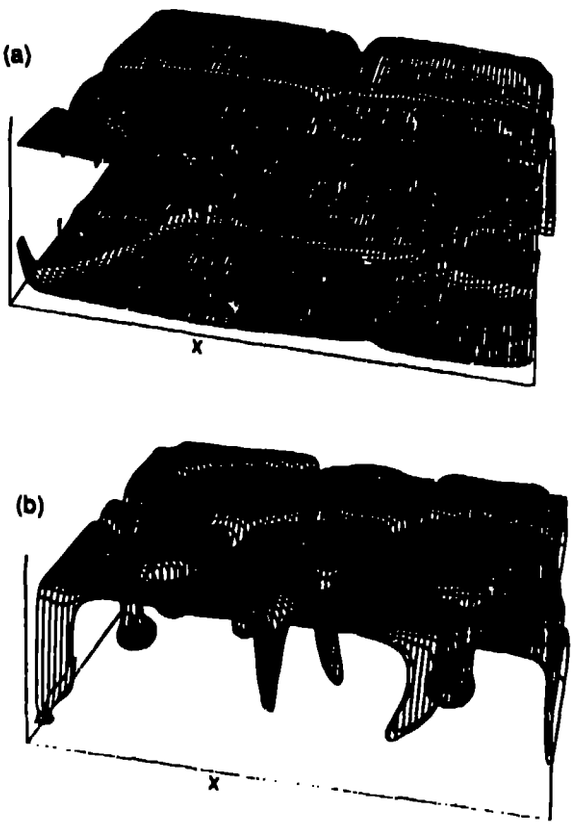

Fig. 2(a) Temperature surfaces of T=0.25 (upper) and T=0.75 (lower) for convection in a 1 x 3 x 3 box at Rayleigh number of 1.5×10^5, no internal heating and no slip upper and lower boundary conditions. Flow is slightly time dependent. (b) Same geometry and boundary conditions, but now with internal heating as well as bottom heating. Pattern is time dependent.

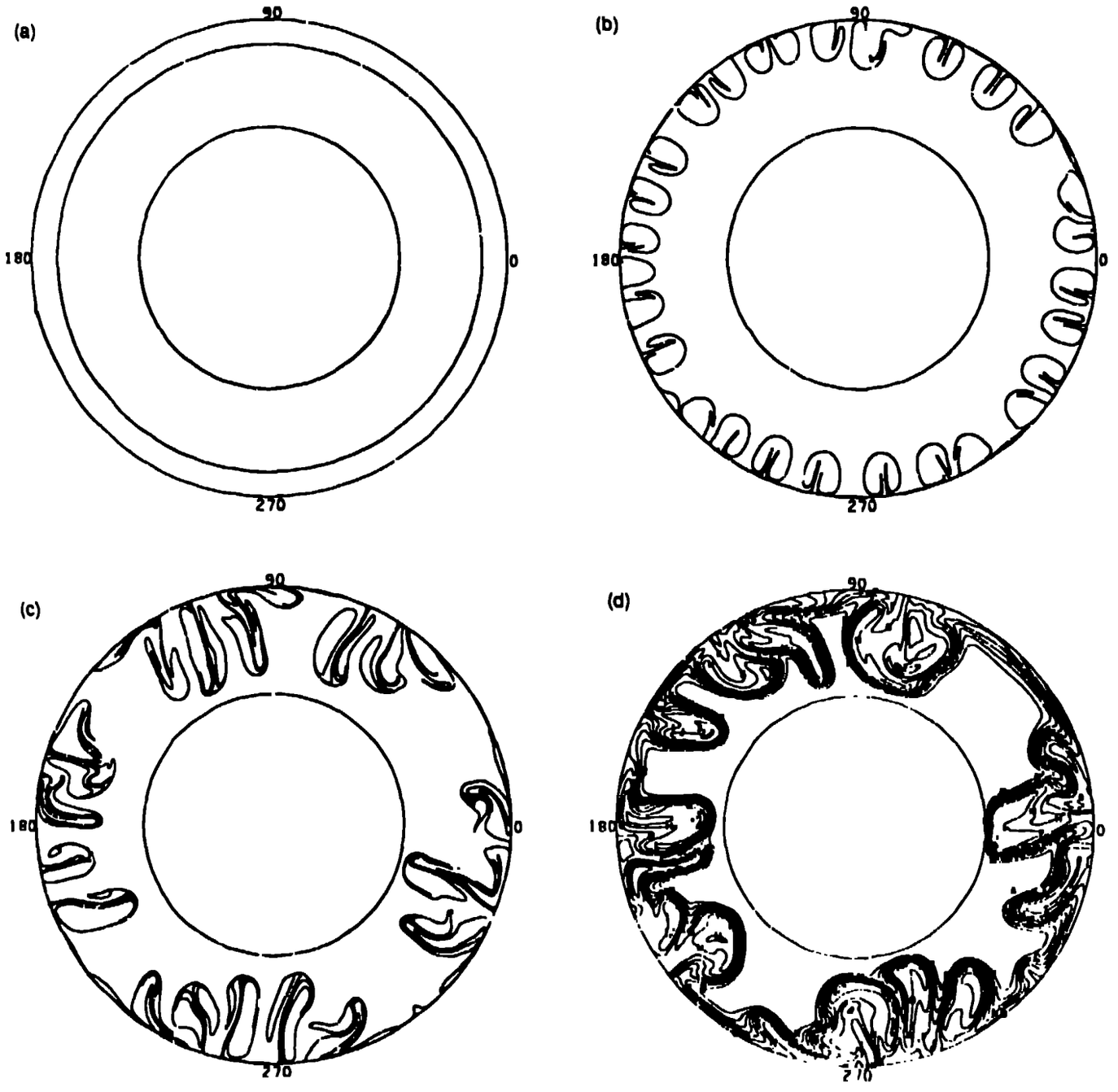

Fig. 3(a) Annular geometry used in penetrative convection studies. Inner and outer radii are in same ratio as the earth. Also shown is initial interface between light and heavy material (light material resides in outermost annular ring). Rayleigh number is 10^7. Mesh consists of 96 cells in the radial direction and 768 in the angular direction. Time in years. Temperature in the annulus initially equal to one in the interior and zero at the surface. (b) Interface between materials at 2 billion years. Convection is occurring only in the outer third of the annulus. (c) Interface at 3 billion years. Convection cells have penetrated deep into the interior. Interface is becoming highly distorted; structure in some locations is thinner than a single mesh cell. (d) Concentration field at 3 billion years for same calculation as (a) - (c) but with finite difference solution of Eqn. (7) alone rather than combined with front tracking. Overall structure is similar to that of (c) but significant differences are developing and small scale structure is quite different.

(2) Penetrative Convection With Two Immiscible Materials

In this example, an initially layered system (light over heavy; $\Delta\rho/\rho = 0.4$) is established in an annulus to represent a possible early earth chemical compositional structure. The temperature profile is initially uniform and hot in the interior ($T = 1$) with a linear decrease to 0 over the outer 6 nodes. A finite difference mesh of 96 cells radially and 768 cells azimuthally is used for the solutions of Eqns. (6) and (7). The Rayleigh number is 10^7, which is believed to be close to the present average earth value. The interest is in knowing when and how large scale convection evolves. Fig. 3a shows the initial location of the interface separating light from heavy material. The subsequent evolution at 2 billion and at 3 billion years, as calculated using front-tracking with the finite difference -spectral method described earlier, are shown in Figs. 3b and 3c. At early times, convection is restricted to the upper part of the mantle. As the interior is cooled, convective motion penetrates farther, and adjacent cells coalesce into larger cells. The interface is getting strongly distorted; some sections are crossing a single mesh cell several times. The pattern in Fig. 3c is to be contrasted with the concentration field shown in Fig. 3d, which shows concentration contours when using only the finite difference solution for Eqn. (7) rather than the front tracking scheme. The sharp interfaces of Fig. 3c separating the two immiscible materials has become diffuse in Fig. 3d. The general features of the flow in both cases are similar, but as time goes on, the one using only the finite difference method begins to deviate more and more because the buoyancy term in Eqn. (1) is diverging from the value provided by the more accurate front-tracking algorithm. By the end of the simulation, the interface has grown to include over 80,000 particles. These results of course depend on the inital conditions chosen. This simulation is intended mainly to demonstrate the value of coupling a front-tracking algorithm to a finite difference solution. Three dimensional calculations using the interface tracking scheme and several species of differing density and viscosity are planned in the future to address the fate of subducting slabs in the vicinity of the earth's 670 km discontinuity.

CONCLUSION

The advent of supercomputers and the combination of various numerical methods to create hybrid schemes is allowing us to simulate 2-D and 3-D models of geophysical convection systems at a level of detail and realism not possible just a few years ago. There are still challenging problems ahead in modeling, such as finding truly efficient methods for including highly variable viscosity, nonlinear rheology, and plate breaking in our earth models. Moving mesh methods, which combine the best features of finite difference and finite element approximations with the advantages of Lagrangian and front tracking algorithms probably hold the most promise for treating these difficult problems.

ACKNOWLEDGEMENT

This work has been supported by the U. S. Department of Energy.

REFERENCES

Christensen, U. R., and Yuen, D. A. 1984, "The Interaction of a Subducting Lithospheric Slab with a Chemical or Phase Boundary," *J. Geophys. Res.*,, Vol. 89, pp. 4389-4402.

Dritschel, D. G.,1988, "Contour Surgery: A Topological Reconnection Scheme for Extended Integrations Using Contour Dynamics," *J. Comp. Physics*, Vol. 77, pp. 240-266.

Gable, C. W.,1989, "Numerical Models of Plate Tectonics and Mantle Convection in Three Dimensions," Ph. D. thesis, Harvard University, Cambridge.

Hirt, C. W., 1968, "Heuristic Stability Theory for Finite-Difference Equations," *J. Comp. Physics*, Vol. 2, pp. 403-411.

Hoffmann, A. W., and Magaritz, M., 1977, "Diffusion of Ca, Sr, Ba and Co in a Basalt Melt: Implications for the Geochemistry of the Mantle," *J. Geophys. Res.*, Vol. 82, pp. 5432-5440.

Margolin, L. G., and Smolarkiewicz, P. K., 1989, "Antidiffusive Velocities for Multipass Donor Cell Advection," Lawrence Livermore National Laboratory report UCID-21866, Dec., 1989.

Ramshaw, J., and Dukowicz, J., 1979, "APACHE: A Generalized-Mesh Eulerian Computer Code for Multicomponent Chemically Reactive Fluid Flow," Los Alamos National Laboratory report LA-7427.

Roache, P. J., 1972, *Computational Fluid Dynamics*, Hermosa Publishers, Albuquerque, NM.

Schafer-Perini, A., Wilson,J. L. and Perini,M., 1990, "Efficient and Accurate Front Tracking for Two-Dimensional Groundwater Flow Models." *Water Resources Research*, in press.

Schafer-Perini, A., and Wilson, J. L., 1990, "Efficient and Accurate Front Tracking for Three-Dimensional Groundwater Flow Models," *Water Resources Research*, in review.

Travis, B. J., Olson, P., and Schubert, G., 1990, "The Transition from Two- Dimensional to Three-Dimensional Planforms in Infinite Prandtl Number Thermal Convection," *J. Fluid Mechanics*, in press.

Travis, B. J., Weinstein, S., and Olsen, P., 1990, "Three-Dimensional Convection Planforms with Internal Heat Generation," *Geophysical Research Letters*, Vol. 17, pp. 243-246.

Weinstein, S., and Olson, P., 1990, "Planforms in Thermal Convection With Internal Heat Sources at Large Rayleigh and Prandtl Numbers," *Geophysical Research Letters*, Vol. 17, pp. 239-242.